This article was downloaded by: [University of Massachusetts, Amherst], [Jacob Harvey]
On: 29 May 2012, At: 08:07
Publisher: Taylor & Francis
Informa Ltd Registered in England and Wales Registered Number: 1072954 Registered office: Mortimer House, 37-41 Mortimer Street, London W1T 3JH, UK

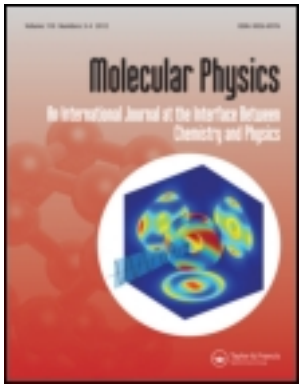

Molecular Physics: An International Journal at the Interface Between Chemistry and Physics
Publication details, including instructions for authors and subscription information:
http://www.tandfonline.com/loi/tmph20

Simulating hydrogen-bond clustering and phase behaviour of imidazole oligomers

Jacob A. Harvey [a], Dipankar Basak [a], Dhandapani Venkataraman [a] & Scott M. Auerbach [a]
[a] Department of Chemistry, University of Massachusetts, Amherst, MA, 01003, USA

Available online: 10 Apr 2012

To cite this article: Jacob A. Harvey, Dipankar Basak, Dhandapani Venkataraman & Scott M. Auerbach (2012): Simulating hydrogen-bond clustering and phase behaviour of imidazole oligomers, Molecular Physics: An International Journal at the Interface Between Chemistry and Physics, 110:9-10, 957-966

To link to this article: http://dx.doi.org/10.1080/00268976.2012.680515

PLEASE SCROLL DOWN FOR ARTICLE

Full terms and conditions of use: http://www.tandfonline.com/page/terms-and-conditions

This article may be used for research, teaching, and private study purposes. Any substantial or systematic reproduction, redistribution, reselling, loan, sub-licensing, systematic supply, or distribution in any form to anyone is expressly forbidden.

The publisher does not give any warranty express or implied or make any representation that the contents will be complete or accurate or up to date. The accuracy of any instructions, formulae, and drug doses should be independently verified with primary sources. The publisher shall not be liable for any loss, actions, claims, proceedings, demand, or costs or damages whatsoever or howsoever caused arising directly or indirectly in connection with or arising out of the use of this material.

Molecular Physics
Vol. 110, Nos. 9–10, 10–20 May 2012, 957–966

Taylor & Francis
Taylor & Francis Group

Downloaded by [University of Massachusetts, Amherst], [Jacob Harvey] at 08:07 29 May 2012

INVITED ARTICLE

Simulating hydrogen-bond clustering and phase behaviour of imidazole oligomers

Jacob A. Harvey, Dipankar Basak, Dhandapani Venkataraman and Scott M. Auerbach*

Department of Chemistry, University of Massachusetts, Amherst, MA, 01003, USA

(*Received 31 January 2012; final version received 9 March 2012*)

We have modelled structures and dynamics of hydrogen bond networks that form from imidazoles tethered to oligomeric aliphatic backbones in crystalline and glassy phases. We have studied the behaviour of oligomers containing 5 or 10 imidazole groups. These systems have been simulated over the range 100–900 K with constant-pressure molecular dynamics using the AMBER 94 forcefield, which was found to show good agreement with *ab initio* calculations on hydrogen bond strengths and imidazole rotational barriers. Hypothetical crystalline solids formed from packed 5-mers and 10-mers melt above 600 K, then form glassy solids upon cooling. Viewing hydrogen bond networks as clusters, we gathered statistics on cluster sizes and percolating pathways as a function of temperature, for comparison with the same quantities extracted from neat imidazole liquid. We have found that, at a given temperature, the glass composed of imidazole 5-mers shows the same hydrogen bond mean cluster size as that from the 10-mer glass, and that this size is consistently larger than that in liquid imidazole. Hydrogen bond clusters were found to percolate across the simulation cell for all glassy and crystalline solids, but not for any imidazole liquid. The apparent activation energy associated with hydrogen bond lifetimes in these glasses (9.3 kJ mol^{-1}) is close to that for the liquid (8.7 kJ mol^{-1}), but is substantially less than that in the crystalline solid (13.3 kJ mol^{-1}). These results indicate that glassy oligomeric solids show a promising mixture of extended hydrogen bond clusters and liquid-like dynamics.

Keywords: hydrogen bonding; clusters; imidazole; oligomers

1. Introduction

Structures and dynamics of hydrogen bond networks play a central role in condensed-phase proton transport in systems as varied as protic liquids [1–5], proton shuttling proteins [6–8], and proton exchange membrane (PEM) fuel cells [9–14]. Many such fuel cells rely on PEM hydration to facilitate proton transport, limiting operation to temperatures below 90°C and requiring complex water management systems [15]. There is thus widespread interest in developing anhydrous PEMs that operate at higher temperatures. Several groups have studied PEMs composed of amphiprotic organic groups tethered to polymeric backbones, only to find exponentially low conductivities [16–21]. This points to a lack of fundamental understanding into how tethering of amphiprotic groups influences hydrogen bond networks in such materials. In the present work, we apply molecular dynamics simulations and cluster statistics to investigate the nature of hydrogen bond networks formed from imidazole groups tethered to oligomeric backbones.

The azole class of organic groups – imidazole, triazoles, benzimidazole, etc. – have received considerable attention [16] as protogenic groups in proton conductors due to their amphiprotic nature, able to donate and accept hydrogen bonds. In general, charge conductivity is the product of mobility and density of charge carriers [22]. The relatively high proton conductivities in azole liquids are believed [2] to arise from enhanced mobility through Grotthuss shuttling [23], a proton transfer process involving collective hydrogen bond fluctuations producing more efficient proton jumps than through the so-called vehicular mechanism [24,25]. In search of PEMs with thermal and mechanical stability as well as high conductivity, several groups have studied azoles tethered to organic polymers [16,26], liquid crystalline supports [21], and inorganic supports [27]. The resulting conductivities for tethered azoles are typically suppressed by orders of magnitude from the corresponding neat liquid values [16]. The precise reasons for this suppression are generally not well understood, but likely involve a mixture of restricted orientational dynamics of azole groups and perturbed hydrogen bond networks.

To investigate the issue of hydrogen bond network topology, Nagamani *et al.* studied polymers with imidazole, 1, 2, 3-triazole, or pyrazole as the

*Corresponding author. Email: auerbach@chem.umass.edu

ISSN 0026–8976 print/ISSN 1362–3028 online
© 2012 Taylor & Francis
http://dx.doi.org/10.1080/00268976.2012.680515
http://www.tandfonline.com

Downloaded by [University of Massachusetts, Amherst], [Jacob Harvey] at 08:07 29 May 2012

amphiprotic group [26]. The structure of imidazole allows the formation of 'linear' hydrogen bonding networks; pyrazole can only produce 'zigzag' networks; and 1, 2, 3-triazole can generate both linear and zigzag networks. Nagamani *et al*. found that polymers with imidazole and 1, 2, 3-triazole exhibit essentially the same conductivity, while the pyrazole-based conductivity is consistently lower by some four orders of magnitude. Although this work shows that proton conductivity is strongly influenced by the structure of hydrogen bonding networks, a molecular-level picture of this influence remains elusive. Density functional theory calculations by Viswanathan *et al*. have shown that the energetics for proton transport along tethered imidazole networks can mimic that in liquid imidazole assuming optimal backbone properties [28]. These DFT calculations also revealed relatively long range proton transport via Grotthuss shuttling (> 40 Å) in extended hydrogen bond networks. However, this work assumed rigid backbones and lacks the effects of solid state packing. In the present work, we perform molecular dynamics simulations of hydrogen bonding networks in imidazole-based solids with explicit backbones. In future work, we will model proton diffusion in such solids to correlate network structure with proton transport.

Below we model imidazoles attached to *oligomeric* backbones in crystalline, glassy, and molten phases. This is similar in spirit to the experimental work of Schuster *et al*. [20], except that we consider oligomers with several imidazoles per oligomer. We hypothesize that proton conducting materials composed of such oligomers – rather than polymers – likely provide all the needed benefits of tethering, including enhanced thermal and mechanical stability. Furthermore, the added conformational freedom available to oligomers makes it easier to simulate the melting and cooling into glassy solids. We do not consider the impact of such tethering on charge carrier density, but rather focus on structures and dynamics that likely impact mobility. We investigate below if oligomer length influences hydrogen bond networks by viewing such networks as clusters, and using established cluster statistics methods [29,30] to keep track of cluster size and spatial extent. We also investigate the likelihood of percolating clusters in these oligomeric solids, and compare these results to those in neat imidazole liquids. Finally, we compare hydrogen bond lifetimes and activation energies between liquid and glassy-oligomeric imidazole, to investigate how tethering impacts hydrogen bond dynamics.

Below we find that glasses composed of 5-mers and 10-mers exhibit essentially the same hydrogen bond cluster statistics, including percolating pathways consistently present below 600 K. In contrast, liquid imidazole exhibits much smaller hydrogen bond clusters and no percolating pathways. Activation energies associated with hydrogen bond breaking were found to be very similar between glassy 5-mers and liquid imidazole, indicating that aspects of liquid-like dynamics are retained in glassy solids. These results indicate that glassy oligomeric solids provide a promising mixture of extended hydrogen bond networks and liquid-like motions.

The remainder of this article is organized as follows: in Section 2 we discuss the model systems, the forcefield and its benchmarking, the cluster and percolation statistics, and the simulation details. In Section 3 we offer results and discussion of the forcefield tests, the thermodynamic states of these systems, hydrogen bond lifetimes, and percolation and cluster statistics. And finally, in Section 4 we provide a summary and concluding remarks.

2. Methods

2.1. *System*

2.1.1. *Oligomers*

We studied oligomers with imidazoles tethered to an aliphatic backbone through propyl linkers as shown in Figure 1. The propyl linker and butyl repeat unit of the backbone were inspired by the electronic structure calculations of Viswanathan *et al*. [28], which showed that propyl groups are the shortest alkyl linkers that allow enough conformational flexibility for strong imidazole–imidazole hydrogen bonding. Viswanathan *et al*. also showed through an implicit model that a backbone repeat distance of ~ 5 Å is optimal for imidazole hydrogen bonding networks; the butyl repeat unit allows such distances. We considered oligomers with $n = 5$ and 10, i.e. 5-mers and 10-mers.

To generate starting three-dimensional structures of hypothetical crystalline solids composed of such oligomers, we began by optimizing a single 5-mer; we then formed a sheet of five such 5-mers such that imidazoles of one oligomer were proximal to the backbone of the next oligomer. Six of these sheets were then stacked in a configuration that allowed π–π stacking between imidazoles in adjacent sheets. This three-dimensional structure – containing a total of 30 oligomers, 150 imidazoles, and 4200 atoms – was then energy-minimized to yield an initial condition for the NpT simulations described below.

System size effects were investigated by simulating a system of 5-mers twice as long in the oligomer axis direction. To produce this system (denoted 'double 5-mer'), the 5-mer system was repeated end-to-end

Downloaded by [University of Massachusetts, Amherst], [Jacob Harvey] at 08:07 29 May 2012

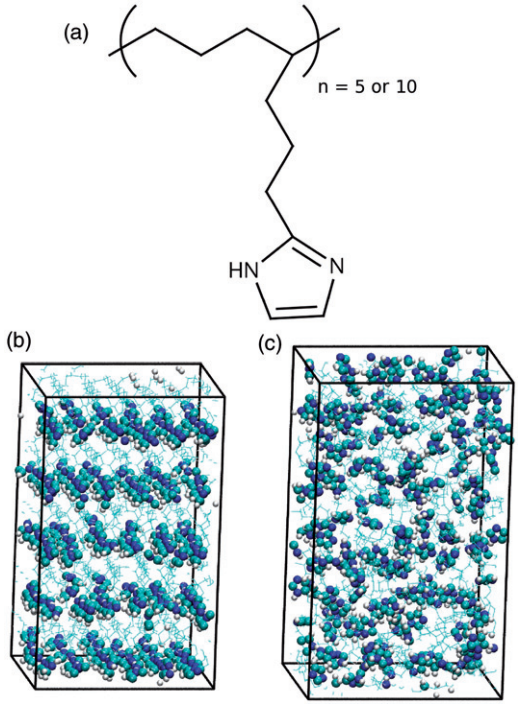

Figure 1. (a) Monomer showing butyl backbone repeat unit, propyl linker, and imidazole. Snapshots from the MD simulations at (b) 300 K and (c) 700 K. The imidazole groups have been emphasized to highlight the order at 300 K and the disorder at 700 K.

such that there is a hydrogen bond between the end of one 5-mer and the beginning of the next, but without a chemical bond between the backbones. The effect of oligomer length was probed by studying a 10-mer system, which is identical to the double 5-mer system except that the two 5-mer backbones are chemically linked in the 10-mer. By comparing the 5-mer and double 5-mer we investigate system size effects for a given oligomer length; while comparing double 5-mer and 10-mer systems probes oligomer length effects for a given system size.

2.1.2. *Liquid imidazole*

The hydrogen bonding properties of simulated liquid imidazole were used as a reference point for interpreting results from the oligomer simulations. To generate an initial structure for simulations of liquid imidazole, the solid imidazole crystal structure with 533 imidazoles was melted and then cooled to various temperatures in the liquid region of the imidazole phase diagram. *NpT* simulations of the liquid were then carried out with the AMBER 94 forcefield to ensure that reasonable liquid densities were obtained.

2.2. *Forcefield*

The AMBER 94 forcefield [31] was used for all simulations. The functional form of the AMBER forcefield is given by:

$$V(X) = \sum_{bonds} \frac{1}{2} k_b (r - r_\circ)^2 + \sum_{angles} \frac{1}{2} k_a (\theta - \theta_\circ)^2 + \sum_{torsions} \frac{1}{2} V_n [1 + \cos(n\omega - \gamma)] + \sum_{j=1}^{N-1} \sum_{i=j+1}^{N} \epsilon_{i,j} \left[\left(\frac{r_{\circ,i,j}}{r_{ij}} \right)^{12} - 2 \left(\frac{r_{\circ,i,j}}{r_{ij}} \right)^{6} \right] + \frac{q_i q_j}{4\pi\epsilon_\circ r_{ij}}. \quad (1)$$

Atomic charges were computed for the monomer (i.e. for imidazole, propyl linker, and butane backbone) by fitting point charges to the electrostatic potential [32,33] obtained using the B3LYP/6-311G(d, p) model chemistry in GAUSSIAN03 [34]. These charges were then repeated in each monomer in the system (see Supporting Information for a list of these charges).

We performed two benchmarks to test the accuracy of the AMBER 94 forcefield in its treatment of hydrogen bonding, for comparison with corresponding electronic structure calculations using the model chemistries indicated below. In the first test, we computed the rotation barrier of an imidazole in a 5-mer with an implicit backbone for computational simplicity, following the work of Viswanathan *et al.* [28]. This implicit backbone involves replacing the butyl repeat unit with a methyl group anchor attached to the end of the propyl linker. The carbons of the five methyl group anchors in the 5-mer were held fixed on a line with a near-neighbour distance of 5 Å. Although this rigid, implicit backbone is a poor approximation of a realistic, flexible backbone, it suffices for testing forcefield accuracy. To compute the rotational barrier, the central imidazole in the 5-mer was rotated 360° in increments of 30° about the C–C bond that connects the central linker to its imidazole. For each value of this dihedral angle, all atoms were allowed to relax except for the implicit backbone anchor carbons, and the atoms of the first and fifth (i.e. edge) monomers. These monomers were held fixed to simulate solid state packing. B3LYP/6-311G(d,p) was used to compute energies and coordinates; the AMBER 94 forcefield was then used to compute potential energies at these coordinates. The results, which are shown in Figure 2 and discussed in more detail below, show that AMBER 94 does a remarkable job of capturing the energetics of this rotation process.

In the second test of AMBER 94, we computed cohesive energies for oligomers of various lengths with propyl linkers and the same implicit backbone as above

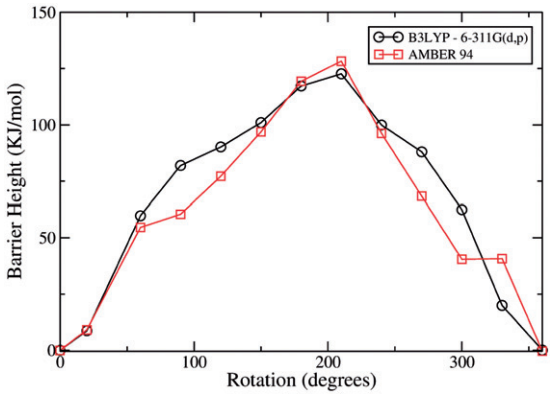

Figure 2. The potential energy associated with rotating the central imidazole in a 5-mer chain, calculated using the AMBER 94 forcefield (squares) and B3LYP/6-311G(d, p) (circles).

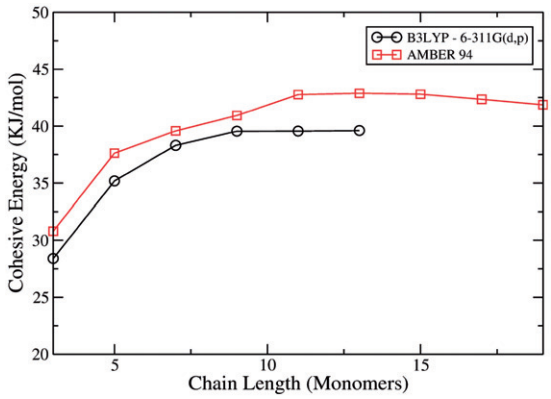

Figure 3. Cohesive energy as a function of oligomer chain length, calculated using AMBER 94 (squares) and B3LYP/6-311G(d, p) (circles).

(5 Å repeat distance). Because of the implicit backbone approximation, this cohesive energy calculation provides an estimate of hydrogen bond strengths in imidazole networks. DFT was used to optimize the energies of odd n-mers (E_n) for $n = 1$ to 13. The DFT cohesive energy ($E_{\mathrm{DFT}} > 0$) of the n-mer was then computed as:

$$E_{\mathrm{DFT}} = \frac{1}{n}(nE_1 - E_n). \tag{2}$$

For these relatively long oligomers, naively applying B3LYP/6-311G(d,p) becomes impractical. Viswanathan *et al.* showed that near-chemical accuracy in hydrogen bond strengths for such systems can be obtained using BLYP/3-21G optimizations followed by BLYP/6-311G(d,p) single point energy corrections [28]. We apply this model chemistry below.

A different but theoretically identical approach was used with AMBER 94 to compute cohesive energies. Using AMBER 94 we calculated single point energies of n-mers using coordinates from DFT optimizations. We then increased the repeat distance of the implicit backbone to extremely large values (~100 Å) and recalculated the energy (E_∞) of the n well-separated and independent monomers. The AMBER cohesive energy (E_{AMBER}) was thus computed as:

$$E_{\mathrm{AMBER}} = \frac{1}{n}(E_\infty - E_n). \tag{3}$$

These cohesive energy calculations, shown in Figure 3 and discussed in more detail below, provide additional support for the notion that AMBER 94 captures the energetics of hydrogen bonding in these imidazole networks.

2.3. *Hydrogen bonds, percolation, and cluster statistics*

Here we describe the methods used to characterize the hydrogen bond structure and dynamics in the systems described above. First we describe the definitions of local quantities such as hydrogen bonds and their lifetimes. Then we outline the treatment of more collective properties such as clusters and percolating pathways. The maximum number of hydrogen bonds equals the number of imidazoles: 150 in the 5-mer system, and 300 in the double 5-mer and 10-mer systems. We report the percentage of hydrogen bonds relative to this maximum, counting a hydrogen bond when an NH···N intermolecular distance is less than 2.5 Å, which is well into the tail of the radial distribution function for such hydrogen bonds under ambient conditions. Statistics for hydrogen bond lifetimes were compiled by recording start and end times for each instance of a hydrogen bond. Mean lifetimes were computed as a function of temperature, and apparent activation energies for hydrogen bond breaking were extracted from crystalline and glassy oligomers, for comparison with neat liquid imidazole.

To complement these local quantities, we compiled statistics on collective properties of the hydrogen bond networks such as cluster sizes and likelihoods of percolating pathways. These collective properties were analysed using established cluster-counting methods involving a connectivity matrix **C** [30]. Elements of the matrix indicate connectivities between imidazoles as follows:

$$C_{ij} = \begin{cases} 1, & \text{if imidazoles } i \text{ and } j \text{ are connected by} \\ & \quad \text{a single hydrogen bond network,} \\ 0, & \text{otherwise.} \end{cases}$$

Downloaded by [University of Massachusetts, Amherst], [Jacob Harvey] at 08:07 29 May 2012

Downloaded by [University of Massachusetts, Amherst], [Jacob Harvey] at 08:07 29 May 2012

The connectivity matrix can be decomposed into direct and indirect terms according to:

$$C_{ij} = C_{ij}^{\text{direct}} + C_{ij}^{\text{indirect}}. \quad (4)$$

The (i, j) element of the direct matrix is unity if imidazoles i and j share a hydrogen bond together, and zero otherwise, thus providing a matrix representation of the local properties described above. The indirect matrix represents the long range nature of hydrogen bond networks, and can be determined by looping over matrix elements and enforcing the following relation:

$$\text{if } C_{ij} = 1 \text{ and } C_{jk} = 1 \text{ then } C_{ik} = 1.$$

In practice this means that if any two columns of $\mathbf{C}^{\text{direct}}$ have non-zero elements in common then the imidazoles that correspond to those columns are directly or indirectly connected and as such exist in the same cluster. The columns are then replaced with the union of the two. This operation is then performed successively until the direct connectivity matrix has been transformed into the full connectivity matrix. As the connectivity matrix is formed we assign an identifying label to each imidazole that belongs to the same cluster. We also keep track of the numbers of imidazoles in each cluster, denoted cluster 'size' which can vary from as small as one to as large as all the imidazoles in the system. In practice, cluster sizes are usually (but not always) smaller than the oligomer size in a given system.

A percolating pathway exists if the cluster label of an imidazole on one 'edge' of the simulation box is the same as the label of an imidazole on the opposite edge of the box. The maximum number of percolating pathways – equal to the number of oligomers in the box (30 or 60) – is used as a reference for reporting the percentage of percolating pathways for each system studied as a function of temperature. There is some ambiguity in assigning 'edge' status to a given imidazole. We (somewhat arbitrarily) define edge imidazoles as those for which at least three of the non-hydrogen atoms are within 4.5 Å of a simulation box edge. This distance is inspired by the rough size (i.e. kinetic diameter) of imidazole.

2.4. *Simulation details*

Molecular dynamics simulations were performed using the DL_Poly_2 simulation package [35]. All simulations were run in the NpT ensemble by using the Melchionna modification of the Hoover algorithm which couples a Nosé–Hoover thermostat and a barostat [36,37]. We used a 1 ps thermostat relaxation time and a 2 ps barostat relaxation time. A 10 Å cutoff was used for the short range interactions, and periodic boundary conditions were applied in all directions with the Ewald summation [38] to calculate long range electrostatic interactions. The Velocity Verlet algorithm was used to integrate Newton's equations of motion with a 1 fs time step [38].

Each run involved equilibration and data collection periods with durations that varied with system size and initial condition (see below). During the equilibration period, atomic velocities were re-scaled every 50 time steps according to Gaussian distributions for the target temperature and mass. Simulations of oligomer systems were performed at temperatures in the range 100–900 K, and those on neat liquid imidazole were carried out in the thermodynamically allowed range of 375–525 K, all at a pressure of 1 atm. We computed two types of isobars for the oligomeric solids, denoted 'heating' and 'cooling' curves. In the heating curve for 5-mers, all simulations were initiated from the optimized hypothetical ordered structure shown in Figure 1(b) (5-mers); they were equilibrated for 10 ns followed by a data collection period of 5 ns. For double 5-mers and 10-mers, each point on the heating curve was initiated with a structure taken from the last temperature run to speed up equilibration for the larger system size. These runs typically involved an equilibration time of 0.6 ns and a data collection period of 2.6 ns. This shorter time was found to provide sufficient statistics because of the larger system size.

In all cooling curves, an equilibrium snapshot from 900 K was used to begin a simulation at 800 K; an equilibrated structure from 800 K was used to initiate the run at 700 K; and so forth. Hysteresis was observed below 700 K, at which point the cooling curve produced glassy solids (Figure 1(c) shows the glassy 5-mer system). For the 5-mer system, points on the cooling curve involved 5 ns of equilibration and another 5 ns of data collection. Double 5-mer and 10-mer cooling simulations involved 0.6 ns of equilibration and 2.6 ns of data collection.

Typical simulations (5-mers, total 15 ns run time) were carried out on our beowulf cluster using 16 2.53 GHz processors (two nodes), requiring roughly 85 CPU hours per temperature. Simulations of the larger system size were carried out with 24 processors and required roughly 50 CPU hours per temperature.

3. Results and discussion

Here we report our results on the tests of AMBER 94 including the calculation of liquid and solid densities; the study of hydrogen bonding probabilities and lifetimes; and on the statistics of clusters and

percolating pathways in neat liquid and oligomeric imidazole systems.

3.1. *AMBER 94 forcefield tests*

Figure 2 shows the imidazole rotation barrier in a 5-mer with an implicit backbone. B3LYP/6-311G(d, p) produced a barrier of 123 kJ mol^{-1}, while the AMBER 94 barrier is 128 kJ mol^{-1}, representing quite acceptable agreement given the relatively simplicity of this forcefield. The magnitude of this barrier deserves some attention. Viswanathan *et al.* found hydrogen bond strengths in imidazole 'proton wires' of order 40 kJ mol^{-1} with this same model chemistry [28]. This hydrogen bond strength is substantially greater than that in water [39] which can be explained by the respective dipole moments (μ(water) = 1.85 D, μ(imidazole) = 3.61 D). Complete rotation of the central imidazole constitutes breaking two hydrogen bonds, thus accounting for ~80 kJ mol^{-1} of these barriers. An additional 4 kJ mol^{-1} can be attributed to the torsional barrier of alkyl groups attached to imidazoles [40]. According to the AMBER 94 calculations, the remainder of the barrier (>40 kJ mol^{-1}) arises mostly from steric repulsions between overlapping NH groups upon rotation. The asymmetry in the barrier is caused by the flanking flexible linker groups, which allow motion of the flanking imidazoles to accommodate the central group rotation. We note that imidazole rotation in actual liquids and oligomeric solids likely occurs with *much* lower barriers; this test case confirms that AMBER 94 captures the energetics of imidazole rotation even under strongly constrained conditions.

Figure 3 shows the cohesive energies for several *n*-mers, comparing DFT and AMBER 94 results. The AMBER 94 forcefield again provides remarkable agreement, consistently within 3–8% of the electronic structure results. These data are rather consistent with imidazole hydrogen bond strengths of order 40 kJ mol^{-1}.

3.2. *Bulk densities of liquid and oligomeric solids*

To test thermodynamic aspects of our model, we present in Figure 4 bulk densities computed along heating and cooling isobars for the 5-mer system, alongside densities of neat liquid imidazole in its liquid temperature regime of its phase diagram. The density we have computed for the neat liquid at 400 K (1.05 g cm^{-3}) agrees quite closely with the experimental value of 1.03 g cm^{-3} measured at 384 K [41]. The temperature dependence of the oligomer density is more shallow than that of the liquid, except for the heating curve between 600–700 K. The precipitous decrease in density in this regime signals the order-to-disorder phase change shown in Figures 1(b) and (c). Cooling the system to temperatures at or below 600 K produces hysteresis in the density, indicating the presence of a glassy solid.

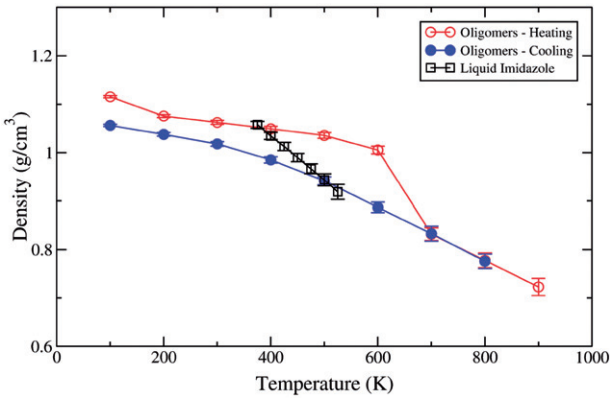

Figure 4. Density of neat liquid imidazole and oligomeric imidazole under 'heating' (open circles) and 'cooling' (closed circles) as a function of temperature. The neat liquid (squares) density agrees well with experiment (see text), and the oligomeric densities are within plausible ranges.

Although no experimental density data exists for the hypothetical oligomeric solids, we can attempt to bracket likely density values. For example, the room temperature density of polybenzimidazole is 1.20 g cm^{-3} [42], while that for 2-butyl, 1H-imidazole is 0.98 g cm^{-3} [43]. We find in Figure 4 room temperature densities intermediate between these two values, suggesting that we have constructed and simulated thermodynamically plausible oligomeric solids.

3.3. *Local hydrogen bonding properties*

Figure 5 shows the percent hydrogen bonds formed at 1 atm as a function of temperature for the neat liquid, the 5-mer glass, and the ordered 5-mer solid. The maximum number of hydrogen bonds in each system is two shared bonds per imidazole, i.e. one distinct hydrogen bond per imidazole. The ordered 5-mer solid is nearly completely hydrogen bonded below 400 K, above which point thermal fluctuations reduce the percentage to about 80%. Above 600 K this value drops precipitously to about 40% as the ordered solid melts, dropping further to about 20% at 900 K, the highest temperature studied. We note that pyrolysis of the organic material would likely ensue at such high temperatures, but because the AMBER 94 is not a

Downloaded by [University of Massachusetts, Amherst], [Jacob Harvey] at 08:07 29 May 2012

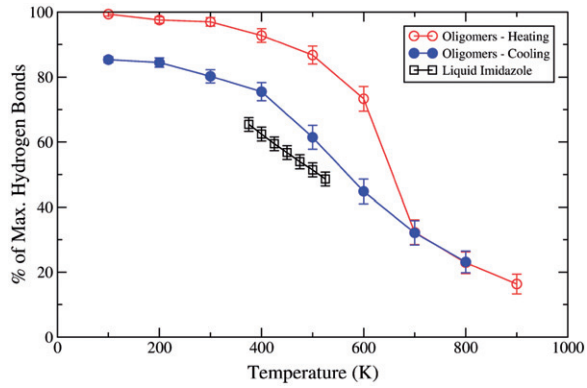

Figure 5. Number of hydrogen bonds as a function of temperature for the neat liquid (squares), the 5-mer glass (closed circles), and the ordered 5-mer (open circles), relative to the maximum value of one per imidazole.

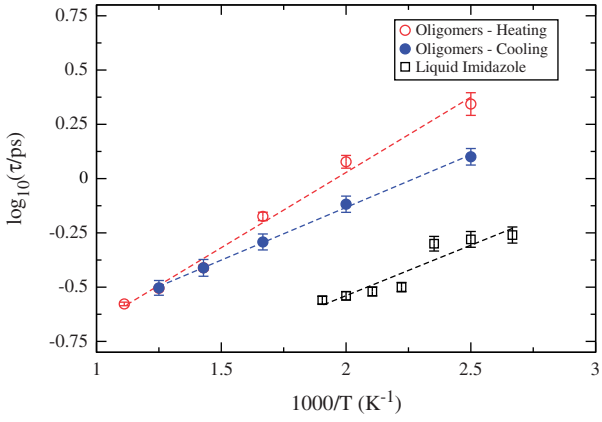

Figure 6. Arrhenius dependence of hydrogen bond lifetimes for the neat imidazole liquid (squares), the 5-mer glass (closed circles), and the ordered 5-mer (open circles), giving apparent activation energies of 8.7, 9.3, and 13.3 kJ mol^{-1}, respectively.

reactive forcefield, we only see thermophysical changes but no thermochemical phenomena. Upon cooling to the glassy 5-mer solid, the percentage of hydrogen bonds reaches a plateau of about 85%. Figure 5 also shows that the glassy solid consistently forms a higher percentage of hydrogen bonds than in the neat liquid at the same temperature.

Figure 6 shows how tethering influences hydrogen bond lifetimes for the neat liquid, glassy 5-mer solid, and ordered 5-mer solid. We see mean hydrogen bond lifetimes on the ps time scale for 5-mer solids, and slightly shorter lifetimes for the neat liquid. Slopes from these Arrhenius plots give apparent activation energies of 8.7 kJ mol^{-1} for the neat liquid, 9.3 kJ mol^{-1} for the 5-mer glass, and 13.3 kJ mol^{-1}

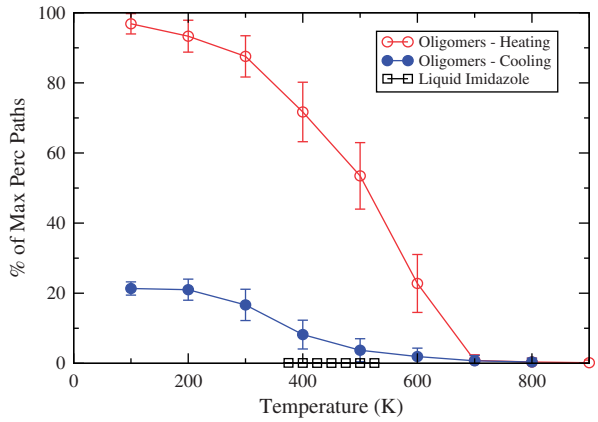

Figure 7. Fraction of percolating pathways for the neat liquid (squares), 5-mer glass (cooling, closed circles), and ordered 5-mer (heating, closed circles) curves. While the 5-mer glass forms few percolating pathways compared to the ordered solid, there is always at least one percolating pathway present in the glass below 700 K.

for the ordered 5-mer solid. These activation energies are all much smaller than the nominal imidazole hydrogen bond strength of 40 kJ mol^{-1} discussed above, suggesting that hydrogen bond breaking/reforming is a concerted process that does not require sustained rupture [4,44,45]. Taken together, Figures 5 and 6 show that tethering imidazoles in an oligomeric glass increases the likelihood of hydrogen bonding, but does not substantially increase the energetics of hydrogen bond breaking as compared to the neat liquid. The question remains, however, whether these systems differ on longer length scales.

3.4. *Percolating pathways*

Figure 7 shows the percent of percolating pathways in the neat liquid, 5-mer glass, and the ordered phase, relative to the maximum number (the number of oligomers = 30) in the simulation. Such pathways involve clusters of hydrogen bonds that extend from one end of the simulation box to the other, providing potentially facile routes for proton transport. While this normalization constant of 30 is not meaningful for the neat liquid, it is moot because the neat liquid never produced a percolating hydrogen bond pathway in any of our simulations.

Comparing Figures 5 and 7 shows that at 600 K, the ordered solid retains about 80% of its hydrogen bonds but only about 20% of its percolating pathways, suggesting that the latter is a much more collective and sensitive property of the hydrogen bond network. The

Downloaded by [University of Massachusetts, Amherst], [Jacob Harvey] at 08:07 29 May 2012

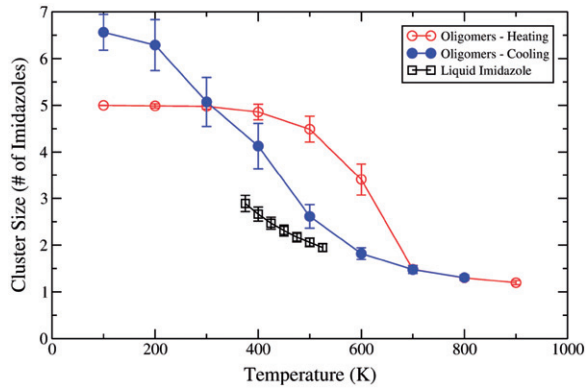

Figure 8. Mean hydrogen bond cluster size as a function of temperature for the neat liquid (squares), 5-mer glass (closed circles) and the ordered 5-mer (open circles). The cold 5-mer glass exhibits the largest cluster sizes due to the formation of tortuous paths.

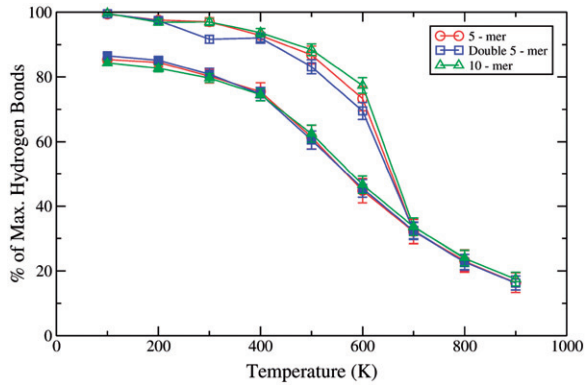

Figure 9. Fraction of hydrogen bonds versus temperature for various system sizes and oligomer lengths. Open symbols denote the heating curves while closed symbols are for the cooling curves.

same picture applies to the 5-mer glass at 300 K: 80% of the hydrogen bonds remain intact but only 20% of the percolating pathways are present. Although upon cooling the glass only reforms about 20% of its possible percolating pathways, this is still a substantial result compared to that for the neat liquid.

3.5. *Cluster statistics*

Figure 8 shows mean cluster size as a function of temperature for the neat liquid, 5-mer glass, and ordered 5-mer solid. The cold, ordered 5-mer solid shows the expected cluster size of 5, which upon melting approaches the minimum value of unity (i.e. few hydrogen bonds). Upon cooling we see the oft-cited hysteresis effect, but surprisingly the cold *glass exhibits larger mean cluster sizes* than does the ordered solid, arising from tortuous paths in the glass as opposed to the linear paths in the ordered solid. In all cases, the hydrogen bond cluster sizes in these oligomeric solids are larger than in the corresponding neat liquid.

3.6. *System size and oligomer length effects*

Figure 9 shows the percent of hydrogen bonds that arise from the heating and cooling curves for the 5-mer, double 5-mer, and 10-mer systems. This shows that neither system size (5-mer versus double 5-mer) nor oligomer length (double 5-mer versus 10-mer) changes this quantity. It remains to be seen if more collective properties such as cluster size are sensitive to system size or oligomer length.

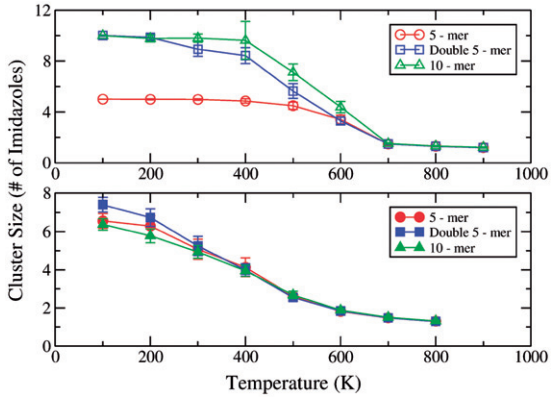

Figure 10. Mean cluster size versus temperature for various system sizes and oligomer lengths. The top graph represents heating curves and the bottom graph represents cooling curves.

Figure 10 shows mean hydrogen bond cluster sizes for the 5-mer, double 5-mer, and 10-mer systems, with heating curves in the top panel and cooling curves in the bottom one. As expected, the double 5-mer and 10-mer ordered systems show cluster sizes around 10, while corresponding 5-mer systems begin at 5. However, upon melting and cooling to produce the glassy versions of these three systems, there is no statistically significant difference in cluster size among the three systems. This result suggests two important conclusions. First, both local (Figure 9) and collective (Figure 10) hydrogen bonding properties are converged with respect to system size in our simulations. Second, and perhaps more important, the effect of tethering on the nature of the hydrogen bonding network has already converged by an oligomer length

Downloaded by [University of Massachusetts, Amherst], [Jacob Harvey] at 08:07 29 May 2012

of 5. This lack of sensitivity suggests that there is little need for synthetic chemists to exert tight control over oligomer length in such systems.

4. Summary and concluding remarks

We have applied molecular dynamics with the AMBER 94 forcefield to model structures and dynamics of hydrogen bond networks that form from imidazoles tethered to oligomeric aliphatic backbones in crystalline and glassy phases. We have studied the behaviour of oligomers containing 5 or 10 imidazole groups, and have compared this behaviour to properties of the neat imidazole liquid. AMBER 94 was found to produce good agreement with DFT calculations on imidazole rotation barriers and hydrogen bond strengths. The oligomeric systems have been simulated over the range 100–900 K with constant-pressure molecular dynamics, and the neat liquid was simulated in its standard liquid region of 375–525 K. The resulting liquid and solid densities show good agreement with available experimental data on imidazole liquid, substituted imidazole liquid, and polybenzimidazole solid.

Local and collective hydrogen bonding properties were extracted from these simulations in two different hypothetical phases: a 'heating' curve initiated from an ordered oligomeric phase that eventually melts above 600 K, and a 'cooling' curve that produces hysteresis through the formation of a glassy oligomeric solid.

For each of these phases, we gathered statistics on hydrogen bond cluster sizes and percolating pathways as a function of temperature, for comparison with the neat imidazole liquid. We have found that the 5-mer and 10-mer glasses show the same hydrogen bond mean cluster size, and that this size is consistently larger than that in liquid imidazole. Hydrogen bond clusters were found to percolate across the simulation cell for all glassy and crystalline solids, but not for any imidazole liquid. The apparent activation energy associated with hydrogen bond lifetimes in these glasses ($9.3\,\mathrm{kJ\,mol^{-1}}$) is close to that for the liquid ($8.7\,\mathrm{kJ\,mol^{-1}}$), but is substantially less than that in the crystalline solid ($13.3\,\mathrm{kJ\,mol^{-1}}$).

These results indicate that glassy oligomeric solids show a promising mixture of extended hydrogen bond clusters and liquid-like dynamics. These oligomer glasses are attractive targets for synthetic chemists because their hydrogen bond properties appear to be relatively insensitive to oligomer length, thus removing the need for tight control over that property.

Future work on these systems include simulating proton diffusion in such solids, studying the effects of different functional groups, and investigating the influence of counterion dynamics in proton transport.

Acknowledgements

This material is based upon work supported by, or in part by, the U.S. Army Research Laboratory and the U.S. Army Research Office under grant number 54635CH. We also thank the members of the UMass Amherst Fueling the Future Center for Chemical Innovation for fruitful discussions. Finally, SMA thanks Prof. William H. Miller, to whom this article is dedicated on the occasion of his becoming a lively septuagenarian, for constant support and inspiration in the endeavour of theoretical chemistry.

References

[1] K. Kreuer, A. Fuchs, M. Ise, M. Spaeth and J. Maier, Electrochim. Acta **43**, 1281 (1998).
[2] H. Chen, T. Yan and G.A. Voth, J. Phys. Chem. A **113**, 4507 (2009).
[3] W. Münch, K.D. Kreuer, W. Silvestri, J. Maier and G. Seifert, Solid State Ionics **145**, 437 (2001).
[4] U.W. Schmitt and G.A. Voth, J. Chem. Phys. **111**, 9361 (1999).
[5] D. Eisenberg and W. Kauzmann, *The Structure and Properties of Water* (Oxford University Press, Oxford, 1969).
[6] S. Iwata, C. Ostermeier, B. Ludwig and H. Michel, Nature **376**, 660 (1995).
[7] D. Marx, ChemPhysChem **7**, 1848 (2006).
[8] J.L.S., Jr and S.A. McLuckey, J. Am. Chem. Soc. **118**, 7390 (1996).
[9] S. Feng and G.A. Voth, J. Phys. Chem. B **115**, 5903 (2011).
[10] S.J. Paddison and R. Paul, Phys. Chem. Chem. Phys. **4**, 1158 (2002).
[11] J.A. Elliot and S.J. Paddison, Phys. Chem. Chem. Phys. **9**, 2602 (2007).
[12] S.S. Jang, V. Molinero, T. Cagin and W.A.G., III, J. Phys. Chem. B **108**, 3149 (2004).
[13] R. Devanathan, A. Venkatnathan and M. Dupuis, J. Phys. Chem. B **111**, 8069 (2007).
[14] R. Devanathan, A. Venkatnathan and M. Dupuis, J. Phys. Chem. B **111**, 13006 (2007).
[15] J. Rozière and D. Jones, Ann. Rev. Mat. Res. **33**, 503 (2003).
[16] K.D. Kreuer, S.J. Paddison, E. Spohr and M. Schuster, Chem. Rev. **104**, 4637 (2004).
[17] M. Schuster, W. Meyer, M. Shuster and K. Kreuer, Chem. Mater. **16**, 329 (2004).
[18] G.R. Goward, M.F.H. Shuster, D. Sebastiani, I. Schnell and H.W. Spies, J. Phys. Chem. B **106**, 9322 (2002).
[19] G. Scharfenberger, W. Meyer, G. Wegner, M. Schuster, K. Kreuer and J. Maier, Fuel Cells **3**, 237 (2006).
[20] M. Shuster, T. Rager, A. Noda, K. Kreuer and J. Maier, Fuel Cells **5**, 355 (2005).

Downloaded by [University of Massachusetts, Amherst], [Jacob Harvey] at 08:07 29 May 2012

[21] D. Basak, S. Christensen, S.K. Surampudi, C. Versek, D.T. Toscano, M.T. Tuominen, R.C. Hayward and D. Venkataraman, Chem. Commun. **47**, 5566 (2011).
[22] E. Barsoukov and J.R. MacDonald, *Impedance Spectroscopy: Theory, Experiment, and Applications* (Wiley, Hoboken, 2005) Hoboken, 2005).
[23] C. de Grotthuss, Ann. Chim **LVVII**, 54 (1806).
[24] N. Agmon, Chem. Phys. Lett. **244**, 456 (1995).
[25] O. Markovitch, H. Chen, S. Izvekov, F. Paesani, G.A. Voth and N. Agmon, J. Phys. Chem. B **112**, 9456 (2008).
[26] C. Nagamani, C. Versek, M. Thorn, M.T. Tuominen and S. Thayumanavan, J. Polym. Sci. **48**, 1851 (2010).
[27] W. Cavalcanti, R. Marschall, P. Tölle, C. Köhler, M. Wark and T. Frauenheim, Fuel Cells **3**, 244 (2008).
[28] U. Viswanathan, D. Basak, D. Venkataraman, J.T. Fermann and S.M. Auerbach, J. Phys. Chem. A **115**, 5423 (2011).
[29] T.L. Hill, J. Chem. Phys. **23**, 617 (1955).
[30] E. Sevick, P. Monson and J. Ottino, J. Chem. Phys. **88**, 1198 (1988).
[31] W.D. Cornell, P. Cieplak, C.I. Bayly, I.R. Gould, J. Kenne M. Merz, D.M. Ferguson, D.C. Spellmeyer, T. Fox, J.W. Caldwell and P.A. Kollman, J. Am. Chem. Soc. **117**, 5179 (1995).
[32] B.H. Besler, K.M.M., Jr and P.A. Kollman, J. Comput. Chem. **11**, 431 (1990).
[33] U.C. Singh and P.A. Kollman, J. Comput. Chem. **5**, 129 (1984).
[34] M.J. Frisch, G.W. Trucks, H.B. Schlegel, G.E. Scuseria, M.A. Robb, J.R. Cheeseman, G. Scalmani, V. Barone, B. Mennucci, G.A. Petersson, H. Nakatsuji, M. Caricato, X. Li, H.P. Hratchian, A.F. Izmaylov, J. Bloino, G. Zheng, J.L. Sonnenberg, M. Hada, M. Ehara, K. Toyota, R. Fukuda, J. Hasegawa, M. Ishida, T. Nakajima, Y. Honda, O. Kitao, H. Nakai, T. Vreven, J.A. Montgomery, Jr., J.E. Peralta, F. Ogliaro, M. Bearpark, J.J. Heyd, E. Brothers, K.N. Kudin, V.N. Staroverov, R. Kobayashi, J. Normand, K. Raghavachari, A. Rendell, J.C. Burant, S.S. Iyengar, J. Tomasi, M. Cossi, N. Rega, J.M. Millam, M. Klene, J.E. Knox, J.B. Cross, V. Bakken, C. Adamo, J. Jaramillo, R. Gomperts, R.E. Stratmann, O. Yazyev, A.J. Austin, R. Cammi, C. Pomelli, J.W. Ochterski, R.L. Martin, K. Morokuma, V.G. Zakrzewski, G.A. Voth, P. Salvador, J.J. Dannenberg, S. Dapprich, A.D. Daniels, . Farkas, J.B. Foresman, J.V. Ortiz, J. Cioslowski, and D.J. Fox, Gaussian 03, Revision A.1 (Gaussian Inc., Wallingford, CT, 2009).
[35] W. Smith and T. Forester, J. Mol. Graphics **14**, 136 (1996).
[36] W.G. Hoover, Phys. Rev. **31**, 1695 (1985).
[37] S. Melchionna, G. Ciccotti and B. Holian, Mol. Phys. **78**, 533 (1993).
[38] M. Allen and D. Tildesley, *Computer Simulations of Liquids* (Clarendon Press, Oxford, 1989) Oxford, 1989).
[39] O. Markovitch and N. Agmon, J. Phys. Chem. A **111**, 2253 (2007).
[40] S.J. Paddison, K.D. Kreuer and J. Maier, Phys. Chem. Chem. Phys. **8**, 4530 (2006).
[41] D. Lide, *Handbook of Chemistry and Physics* (CRC Press, Boca Raton, 2007) Boca Raton, 2007).
[42] J. Brandrup, E.H. Immergut, E.A. Grulke, A. Abe and D.R. Bloch, *Polymer Handbook*, 4th ed (Wiley, Hoboken, NJ, 2005).
[43] ACD/HNMR Predictor, version 7.03 (Advanced Chemistry Development, Inc., Toronto, ON, Canada, 2003). See <www.acdlabs.com>.
[44] F.W. Starr, J.K. Nielsen and H.E. Stanley, Phys. Rev. E **62**, 579 (2000).
[45] A. Luzar, J. Chem. Phys. **113**, 10663 (2000).

Downloaded by [University of Massachusetts, Amherst], [Jacob Harvey] at 08:07 29 May 2012